Commissionning MATISSE operation and performances

Romain G. Petrov*[a], Fatmé Allouche[a], Alexis Matter[a], Anthony Meilland[a], Stéphane Lagarde[a], Philippe Bério[a], Pierre Cruzalèbes[a], Florentin Millour[a], Sylvie Robbe-Dubois[a], Walter Jaffe[b], Karl-Heinz Hofmann[c], Jozsef Varga[b], Dieter Schertl[c], Leonard Burtscher[b], Klaus Meisenheimer[d], Alain Chelli[a], Gérard Zins[e], Julien Woillez[e], Markus Schöller[e] and Bruno Lopez[a].

[a]Laboratoire Lagrange, Université Côte d'Azur, Observatoire de la Côte d'Azur, CNRS, Boulevard de l'Observatoire, CS 34229, 06304 Nice Cedex 4, France.

[b]Leiden Observatory, Leiden University, Niels Bohrweg 2, NL-2333 CA Leiden, the Netherlands.

[c]Max-Planck-Institut für Radioastronomie, Auf dem Hügel 69, D-53121 Bonn, Germany.

[d]Max Planck Institute für Astronomy, Königstuhl 17, D-69117 Heidelberg, Germany.

European Southern Observatory Headquarters, Karl-Schwarzschild-Straβe 2, 85748 Garching bei München, Germany.

ABSTRACT

MATISSE, the VLTI spectro-interferometric L, M and N bands imager, has been commissioned from March 2018 to March 2020. In N, its performances per baseline are worth those of its predecessor MIDI but it gives 6 baselines and 4 closure phases at once. It is the first spectro-interferometer in the L and M bands and that enhances its sensitivity and opens a new window to all its science programs. MATISSE has produced its first images and has performances better than the specifications set by its core science programs on YSOs, AGNs and Stellar and Planetary Physics. It is already offered to the ESO General User. Analyzing thousands of commissioning measurements allows to predict correctly the performances of MATISSE in terms of measurement precision and calibration accuracy. We discuss the MATISSE standalone performance analysis and its validation and give also the first results of the GRA4MAT combination of the GRAVITY fringe tracker with MATISSE observations.

Keywords: Astronomy, Instrumentation, Optical long baseline interferometry, Thermal Infrared, Spectro-interferometry, Very Large Telescope Interferometer, VLTI, MATISSE.

1. INTRODUCTION

The Very Large Telescope Interferometer (VLTI) is currently the long baseline optical interferometer in operation with the largest collecting area and the highest sensitivity. It combines 4 fixed Unit Telescopes (UTs) with 8m diameter or 4 relocatable Auxiliary Telescopes with 1.8 m diameter. Its longest baseline is currently of 135 m and will soon be extended for ATs to the maximum value of 200 m allowed by the size of the platform at the top of mount Paranal [1]. The VLTI features two 2nd generation instruments open the "General User", GRAVITY in the K band [2,3] and MATISSE in the mid infrared covering the L, M and N bands from 3 to 13 μm [4,5]. GRAVITY contains a fringe tracker, the GFT that can be also used to stabilize the fringes recorded by MATISSE in the so called GRA4MAT (for **GRA**VITY for **MAT**ISSE) mode.

MATISSE has been installed on the VLTI at the beginning of 2018 and has been included in the VLT(I) call for proposals for the first time in September 2018. Observations in open time started in April 2019. The first science results have just been published [6,7] and many others are in the final steps of redaction. The commissionning of MATISSE has started in March 2018 and was scheduled to be concluded in May 2020. In spite of the delay in the last two commissioning runs scheduled in spring 2020 and postponed by the Paranal shutdown due to the covid-19 crisis, the analysis of MATISSE performances is nearly complete. This paper presents the MATISSE performance analysis method and the key results that the General-User should have in mind when (s)he wants to analyze the feasibility and the potential of an observing proposal. The limiting performances given here are very close to these offered in the ESO Call for Proposals (CfP) and this paper is aimed at explaining how they have been obtained and how they can be interpreted and developed.

The main science goals of MATISSE are described in [5] and [8]. They are mainly based on angular measurements and ideally images of dust and molecules with temperatures ranging from 200 to 1500 K. The very broad spectral coverage of MATISSE offers unique constraints on the temperature distribution and mineralogy of the dust in YSOs and AGNs. In the L band it has also access to a large collection of ionized hydrogen lines that would be decisive for the gas dust connection in YSOs, AGNs and active starts with circumstellar environments.

This paper focusses on the performances and limitations of MATISSE standalone as well as in combination with the GFT. However, it is worth having in mind that as a VLTI instrument, MATISSE is also limited by the Adaptive Optics of the VLTI, which sets a V limiting magnitude (NAOMI on ATs with V_{lim}~12 and MACAO on UTs with V_{lim}~14) and by the necessity to track the images in the focal laboratory in spite of the drifts introduced by the long airpath in the delay line tunnels. This set a K band limiting magnitude even when the GFT is not used.

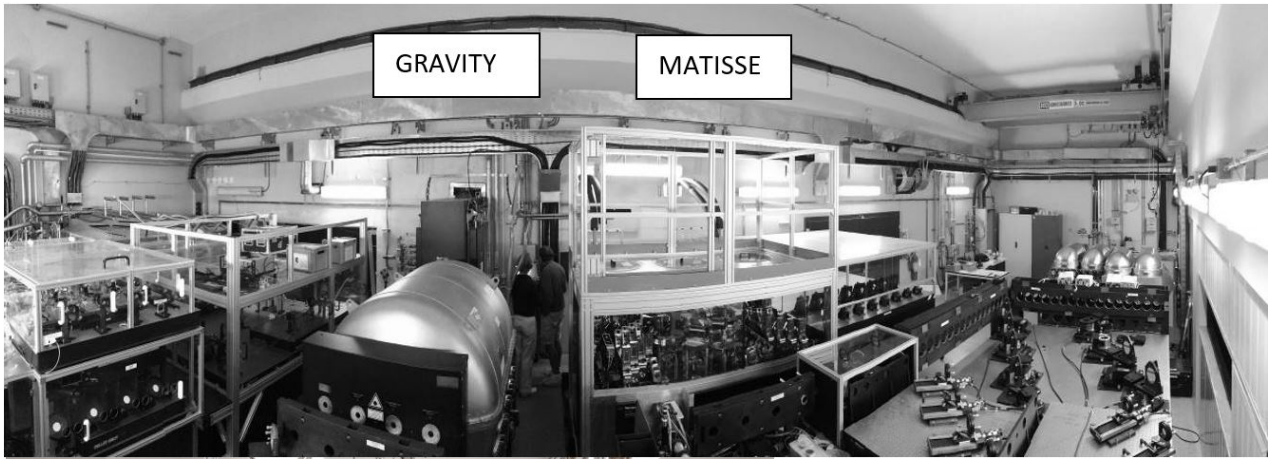

Figure 1. MATISSE (center right) and GRAVITY (center left) in the VLTI focal laboratory.

In section 2 we describe MATISSE and its measurements in order to introduce the way their errors depend from the key instrument parameters. section 3 gives the method to compute and validate the fundamental noise effect on the precision of all measurements. It also describes the calibration errors that affect the accuracy of the visibility and closure phase. Section 4 describes the combination of all these factors in a global performance estimate and shows how this global performance estimate can be validated before giving a synthesis of the performances of MATISSE. Finally, section 5 describes the performance improvement permitted by the GFT on ATs.

2. MATISSE

2.1 Instrument concept and key features

MATISSE is mid infrared imaging spectro-interferometer covering the L, M and N spectral bands, respectively from 2.9 to 4.1 µm, 4.5 to 5 µm and 8 to 13 µm. These spectral bands and the maximum current baseline of the VLTI corresponds to resolutions ranging from 4.5 to 15 milliarcseconds (mas). It is based on an all-in-one concept, similar to this of the first-generation instrument AMBER [9]. All beams are focused inside a common Airy disk that contains 6 fringe patterns, one for each baseline. The fringe patterns are separated in Fourier space by the a non-redundant spacing on the internal pupils in MATISSE. The fringed Airy disk is dispersed by a spectrograph in the direction perpendicular to the internal baselines yielding a dispersed fringe interferogram in a x-λ frame. This interferogram can be completed by individual dispersed photometric beams, each containing the flux and the spectrum of the source seen by each individual aperture.

MATISSE is divided in 3 main components that are the Warm Optics table and the L-M and N band cryostats.

The Warm Optics components shape the beams that must be injected in the cryostats to ensure the proper sampling of the fringes and photometric beams. They co-align MATISSE with the VLTI. They split the light between the L-M and the N bands. They include a reference source that is used for the automatic alignment of all MATISSE components and for the cophasing of all MATISSE beams. They also contain two devices intended to improve the precision of MATISSE measurements.

The Beam Commutation Device (BCD) [10] switches beams 1-2 and 3-4 in 2-1 and 4-3 without loss of alignment or cophasing and in less than 4 seconds. This operation allows to invert all MATISSE closure phases and the differential phases on baselines 1-2 and 3-4 without changing their instrumental component. Then the subtraction of measures with different BCD setups allows to eliminate the instrument errors on the closure and relevant differential phases that vary slower than the BCD calibration cycle, that is typically based on one commutation per mn. This removes the closure phase and differential phase errors resulting from the small evolution of the detector and the residual cross talks between beams and baselines.

The fast OPD modulation of each beam during the piston coherence time of the atmosphere is used to eliminate the contamination of the fringe peaks by the fast variations of the background in the N band. The modulation cycle is executed in 240 ms over 10 N band frames of 20 ms. The modulation amplitudes on each beam allow to demodulate each baseline individually while leaving all other baselines and the photometric low frequency component modulated by a zero-mean signal.

Each one of the Cold Optics cryostats contains a spatial filtering using pinholes and pupil masks that allow MATISSE to be very close to a single mode beam combiner. The L-M band and the N band spectrograph allow the following spectral resolutions.

Table 1. Spectral modes and resolutions of MATISSE

Spectral Mode	Wavelength range	Resolution	Pixels per λ/D
LR-LM	2.9-5 µm	31.5	5 (at 3.5 µm)
MR-LM	2.9-5 µm	499	
HR-L	2.9-4.1 µm	979	
VHR-LM	3.9-5 µm	3370	7 (at 4.7 µm)
LR-N	8-13 µm	31.5	7 (at 10.5 µm)
HR-N	8-13 µm	218	

The LM spectrograph uses and Hawaii-2 detector with 2048x2048 pixels that can be used in a "slow-read" mode with a detector read out noise of about 15 e^- per pixel and per read and a fast "read-mode" of about 75 e^- per pixel and per read. The "fast-read" mode is used only in low spectral resolution (LR-LM) for targets brighter than ~300 Jy in L to avoid detector saturation. In "slow-read" mode the spectral window that can be read in an atmospheric coherence time (less than 120 ms in L) is of 0.2 µm in MR-LM and 0.1 µm in HR-L. Reading the full Hawaii detector needs nearly 1 s and this can be used only when an external fringe tracker stabilizes the fringes observed by MATISSE.

The N band spectrograph contains an Aquarius 2048x2048 detector. In low spectral resolution (LR-N) the frame time is set to 20 ms to avoid saturation by the thermal background. In "high" (HR-N) spectral resolution a frame time of 75 ms allows to read the full spectral 8-13 µm window.

2.2 Matisse measurements

Like any spectro-interferometric instrument since AMBER [9], MATISSE yields the following measurements:

- The complex coherent flux as a function of wavelength $C_{ij}(\lambda)$ for each baseline B_{ij}.

$$C_{ij}(\lambda) = \langle \hat{I}(B_{ij}/\lambda, \lambda) \rangle = \sqrt{n_i(\lambda) n_j(\lambda)} V_{ij}(\lambda) e^{i\varphi_{ij}(\lambda)}$$

where $\hat{I}(B_{ij}/\lambda, \lambda)$ is the Fourier transform of the interferogram $I(x, \lambda)$ at the spatial frequency B_{ij}/λ, $n_i(\lambda)$ is the flux contribution of beam i to the interferogram and $V_{ij}(\lambda)$ and $\varphi_{ij}(\lambda)$ are the modulus and phase of the complex visibility on the baseline ij at the wavelength λ. As $\varphi_{ij}(\lambda)$ randomly changes because of the atmospheric piston, the complex coherent flux can be integrated beyond the atmospheric coherence time only the phase delay is measured and corrected in real time either from MATISSE data itself of from an external fringe tracker. When this is impossible, we can use the phase independent squared modulus of the complex coherent flux

$$|C_{ij}(\lambda)|^2 = < |FT[I_{ij}(\lambda)]|^2 > = n_i(\lambda) n_j(\lambda) V_{ij}(\lambda)$$

- The source spectrum $S(\lambda)$ can be obtained from the photometric measurements:

$$S(\lambda) = \frac{\sum_i < n_i(\lambda) >}{\sum_i < n_i(\lambda_C) >}$$

where λ_C represents a spectral channel in the continuum.

- The source visibility $V_{*ij}(\lambda)$ can be obtained from a combination of the coherent flux and photometric measurements

$$V_{*ij}(\lambda) = \frac{|C_{ij}(\lambda)|}{V_{Iij}(\lambda)\sqrt{< n_i(\lambda) n_j(\lambda) >}}$$

where $V_{Iij}(\lambda)$ is the instrumental visibility. As $V_{Iij}(\lambda)$ can change quite rapidly with seeing and also instrument features such as vibrations in the VLTI and misalignment, it is necessary to use a calibration source with known $V_{*ij}(\lambda)$ to measure $V_{Iij}(\lambda)$ and hence obtain an accurate measure of $V_{*ij}(\lambda)$ on the science source.

MATISSE does not have access to an absolute phase reference (but for the very specific and rare case of a calibrator close enough to the science to appear in the same MATISSE field). It must use the source closure phase and the color differential phase.

- The closure phase is deduced from the coherent flux bispectrum

$$\psi_{ijk}(\lambda) = arg\left[C_{ij}(\lambda) C_{jk}(\lambda) C_{ki}(\lambda)\right]$$

In theory that closure phase is independent of instrumental features in a single mode experiment. In practice there is an instrumental closure phase due to cross-talks between beams and baselines [11]

$$\psi_{ijk}(\lambda) = \psi_{*ijk}(\lambda) + \psi_{Iijk}(\lambda)$$

The instrumental term $\psi_{Iijk}(\lambda)$ can be calibrated with a calibrator or using the BCD that allows to exchange i and j before entering MATISSE. We then have two measurements with different BCD setups:

$$\psi_{OUTijk}(\lambda) = \psi_{*ijk}(\lambda) + \psi_{Iijk}(\lambda)$$

$$\psi_{INijk}(\lambda) = \psi_{*jik}(\lambda) + \psi_{Iijk}(\lambda) = -\psi_{*ijk}(\lambda) + \psi_{Iijk}(\lambda)$$

$$\psi_{*ijk}(\lambda) = \frac{\psi_{OUTijk}(\lambda) - \psi_{INijk}(\lambda)}{2}$$

- The differential phase is the difference between the phase in a given spectral channel and the phase in a reference channel usually obtained from an average of the coherent flux over wavelength.

$$\phi_{D_{ij}}(\lambda) = arg\left[C_{ij}(\lambda)\left\langle C_{ij}^*(\lambda)\right\rangle_\lambda\right] - 2\pi P_{ij}(\lambda)/\lambda$$

where $P_{ij}(\lambda)$ is the residual chromatic group delay estimated from a fit of $arg\left[C_{ij}(\lambda)\left\langle C_{ij}^*(\lambda)\right\rangle_\lambda\right]$, ideally only on channels where the source is known or unresolved, like for example the continuum on each side of an emission line. To estimate the differential phase on large spectral intervals, for example in low resolution observations, we need to calibrate the chromatic group delay $P_{ij}(\lambda)$ from a calibrator and a model of the variation of the air refractive index $n(\lambda, T, p, H)$ with temperature, pressure and humidity.

- The differential visibility is a self-referenced visibility measurement given by

$$\phi_{D_{ij}}(\lambda) = \frac{\Re\left[C_{ij}(\lambda)\left\langle C_{ij}^*(\lambda)\right\rangle_\lambda\right]}{\left\langle |C_{ij}(\lambda)|^2\right\rangle_\lambda}$$

2.3 Observing mode

The modes of MATISSE are set by the method used to calibrate the photometry. In the SiPhot (**Si**multaneous **Pho**tometry), a third of each beam is deflected to a photometric beam that appears on the same detector frame than the interferometric beam. In L, like in K with AMBER, there are fast photometric variations introduced by the fluctuation of the Strehl ratio of the partially correcting adaptive optics and the amplitude of these variations is strongly seeing dependent. On the other hand the background variations are fainter and slower and it should be possible to estimate them from a record of the sky

background before and after the interferometric observation. The HighSens (**High Sens**itivity) has been inspired by MIDI. In this mode all the flux is concentrated in the interferometric channel and the photometry is analyzed sequentially by closing all beams but one. The HighSens mode main justification is that MIDI showed that a lot of spatial useful spatial information can be obtained from the coherent flux alone which give access to the many sources that are too faint for good photometric and hence absolute visibility measurements while they are bright enough for coherent flux estimates. The difference comes from the fact that the strong and very variable background in N has no spatial coherence. The coherent flux SNR depends from the background photon noise but it is almost unsensitive to the changes in background intensity that dominated the photometric measurements. In HighSens the source photometry is estimated sequentially, and the background is eliminated by telescope chopping. That source photometry is sensitive to changes in AO performances that are quite limited in the N band.

MATISSE can use both SiPhot and HighSens in the two cryostats. However, the tests of MATISSE in laboratory showed that the SiPhot mode is hardly applicable to the Aquarius detector that has a linearity and a systematic noise which can be correctly calibrated only in a small flux range and on the same pixels.

We therefore decided to use MATISSE in the so-called Hybrid mode:

- The L-M cryostat is set in SiPhot mode and records interferometric and photometric channels simultaneously
- The N cryostat is in HighSens mode and records only the interferometric channel
- The so-called *interferometric* observation is executed without chopping. It yields interferometric and photometric observations without chopping in L and M and interferometric observations without chopping in N.
    - The standard MATISSE Observing Block (OB) contains 4 exposures of 1 mn, each in one of the 4 BCD configurations (in-in, in-out, out-in and out-out)
- During the so-called *photometric* observation, we record 8 exposures with all N band shutters but one closed with chopping.
    - The photometry of each beam is measured in N with chopping and on the interferometric channel pixels with the corresponding BCD in position “in” and in position “out”
    - During these exposures, the L-M detector records the interferometric and photometric channels with chopping.

2.4 Standard Observing Block

The standard MATISSE OB contains:

- the telescopes preset, which includes pointing, finding a guide star and locking the active optics for the UTs and finally closing the AO loops;
- the acquisition of the images in the VLTI focal laboratory and the closing of the loop for image tracking in the laboratory (called “Coude Laboratory Guiding”);
- the preset of the Delay Lines;
- the acquisition of the fringes by MATISSE or by the GRAVITY Fringe Tracker;
- 2 exposures of 30 s on the sky (one with each BCD position)
- 4 exposures of 1 mn on target without chopping (the N band interferometric exposures)
    - that are also L-M band interferometric and photometric exposures without chopping
- 8 exposures of 1 mn on target with chopping (the N band photometric exposures)
    - that are also L-M band interferometric and photometric exposures with chopping

Given the small overheads between exposure, the minimum duration of this standard OB is 20 mn. ESO proposes a conservative but rather realistic average duration of 25 mn.

3. PERFORMANCE ANALYSIS

3.1 Performance criteria

The limits of MATISSE are set by many VLTI parameters such as the limiting magnitude in V to close the loop of the adaptive optics (V~12 with NAOMI on ATs and V~14 with MACAO on UTs) and the K band limiting magnitude for image tracking in the VLTI focal laboratory. The parameters specific to MATISSE are its capability to acquire images and fringes either in L or in N and to maintain the fringes near the center of the coherence length with its internal group delay tracker. Finally, MATISSE observations are useful only if the data can be processed and provide good quality measurements. We found that the last criteria is by far the most demanding and we agreed with ESO that the MATISSE

sensitivity limit are the coherent fluxes in Jy that allow the following precision or accuracy on each measure par spectral channel and per mn of observation.

- Visibility accuracy: $\sigma_V = 0.1$
- Closure phase accuracy: $\sigma_\psi = 5°$
- Differential phase precision: $\sigma_\varphi = 4°$
- Coherent flux SNR: $C/\sigma_C = 10$

These criteria are quite demanding. Better performances can be obtained by binning spectral channels to obtain broad band observations or by combining several observations. However, users should keep in mind that the precision of measures can usually be improved like the square root of the number of exposures, i.e. here $\sqrt{obs\ time\ in\ mn}$ but calibration errors can be improved only with the square root of the number of calibration cycles i.e. typically $\sqrt{obs\ time\ in\ h}$ for the most demanding absolute visibility calibration.

Note also that obtaining the above visibility and closure phase accuracy allows to retrieve images of resolved targets as soon as the u-v coverage is sufficient, while coherent flux and differential measures allow only model dependent angular constraints on the source, at least with the current state-of-the-art image reconstruction algorithms.

In the next sections we will analyze the fundamental noise error that affect the precision of all measurements, the broad band seeing dependent and flux independent calibration errors that affect the accuracy of the visibility and closure phase and the flux dependent broad band photometric calibration error that affects only the visibility.

3.2 Fundamental noise computation

All MATISSE measurements are derived from the complex coherent flux estimates $C_{ij}(\lambda)$. The error on the coherent flux is set by the fundamental noises that are the source and the background photon noise and the detector noises that in MATISSE are dominated by the Read-Out Noise. The variance of the coherent flux per spectral channel and per frame is given by:

$$\sigma^2_{C_{ij}} = N_p\sigma_R^2 + \sum_{i=1}^{N_T}(n_{*i}+n_{Bi})$$

with n_{*i} and n_{Bi} are the numbers of source and background photons in beam i, N_T is the number of telescopes, N_p the number of pixels to analyze the signal and σ_R^2 the variance of the read-out-noise. The coherent flux SNR per channel and per frame is:

$$SNR_{C_{ij1}} = \frac{C_{ij}}{\sigma_{C_{ij}}} = \frac{\sqrt{n_{i*}n_{j*}}V_{ij}}{\sqrt{N_p\sigma_R^2 + \sum_{i=1}^{N_T}(n_{*i}+n_{Bi})}}$$

When N_λ spectral channels and N_F frames are added coherently, the coherent flux SNR becomes

$$SNR_{C_{ij}} = SNR_{C_{ij1}}\sqrt{N_\lambda N_F}$$

An incoherent integration of channels or frames, i.e. an addition of interferogram power spectrum would yield

$$SNR_{C^2_{ij}} = \frac{(SNR_{C_{ij}})^2}{\sqrt{N_\lambda N_F\left[1 + 2(SNR_{C_{ij}})^2\right]}}$$

which becomes extremely inefficient when $SNR_{C_{ij}} < 1$.

The phase of the coherent flux has a precision

$$\sigma_{\varphi_{ij}} \simeq \frac{1}{\sqrt{2}SNR_{C_{ij}}}$$

This approximation is correct up to $\sigma_{\varphi_{ij}} \simeq 1$ rad. It is a good approximation of the fundamental error on the differential phase, as the errors introduced by the much broader reference channel can generally be neglected.

When the coherent flux phase precision per frame $\sigma_{\varphi_{ij1}} < 1rad$ it is easy to show that the closure phase precision is given by

$$\sigma^2_{\psi_{ijk}} \simeq \sigma^2_{\varphi_{ij}} + \sigma^2_{\varphi_{jk}} + \sigma^2_{\varphi_{ki}} \simeq 3\sigma^2_\varphi$$

When $\sigma_{\varphi_{ij1}} > 1rad$ the closure phase error has a more complex expression. We have found that a two terms development fits our measures estimates with a sufficient accuracy.

$$\sigma_\psi = \sigma_\varphi\sqrt{3} + \alpha\sigma^3_\varphi$$

Where α is a constant for a given MATISSE set-up that is usually set from the measured dispersion of the estimators. The closure phase precision very rapidly decreases below the $\sigma_{\varphi_{ij1}} = 1rad$ limit.

It is therefore critical to use the maximum number of channels and frames that can be coherently integrated. In the following we will give the results for coherent binning of the spectral columns in one spectral channel and for coherent integration of frames over the atmospheric coherence time.

The absolute visibility is deduced from the coherent flux through a photometric correction$V_{ij}(\lambda) = C_{ij}/\sqrt{n_{i*}n_{j*}}$ and its fundamental noise also depends from the precision of the estimates of n_{i*} and n_{j*}:

$$\sigma_{V_{ij}^2} = V_{ij}^2 \left(\frac{\sigma_{C_{ij}^2}^2}{C_{ij}^2} + \frac{\sigma_{n_i}^2}{{n_i}^2} + \frac{\sigma_{n_j}^2}{{n_j}^2} \right)^{1/2}$$

3.3 Fundamental noise measurement

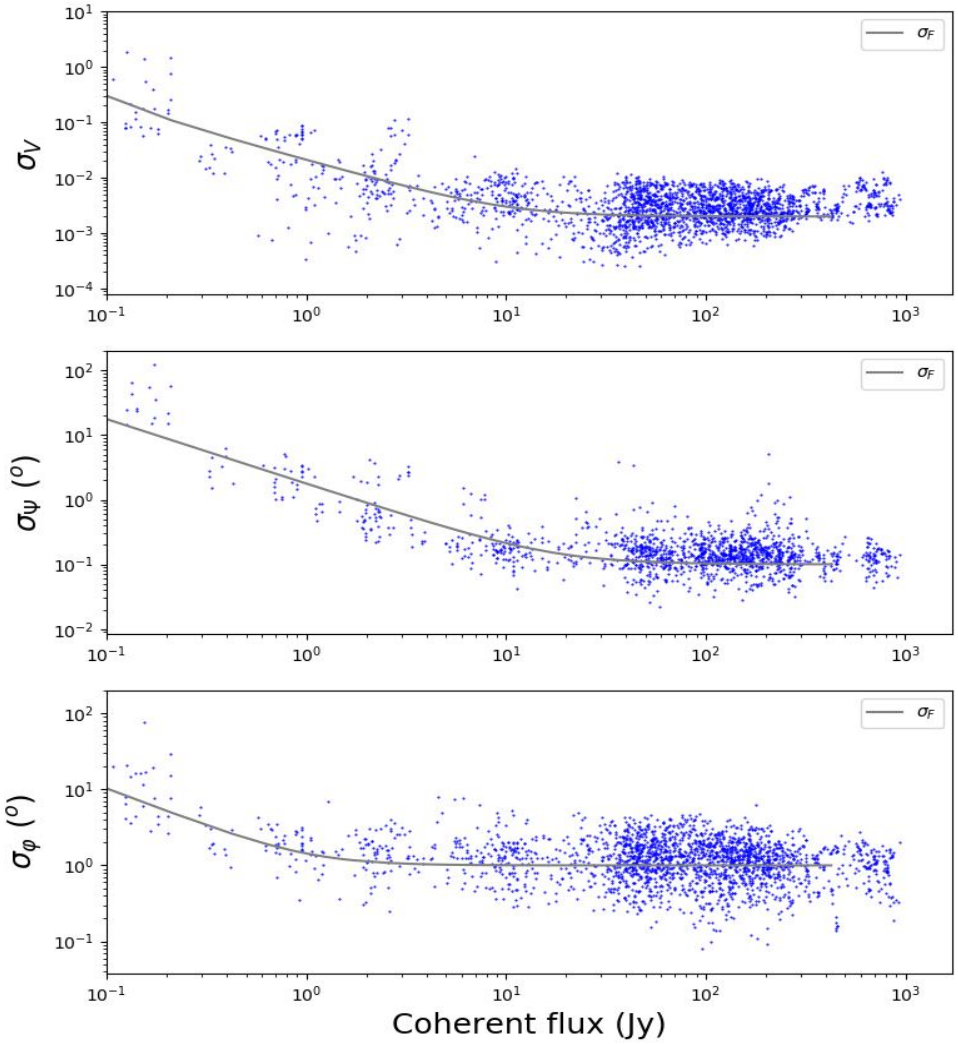

Figure 2. Illustration of the fundamental noise measurement and prediction in the case of L band observations at low spectral resolution with the ATs. We plot the measured fundamental noise per spectral channel (blue dots) as a function of the source coherent flux for the visibility (top), the closure phase (middle) and the differential phase (bottom). The grey line shows the value of the noise prediction given by the formulas in section 3.2. In these plots we merge all baselines, AT configurations and seeing conditions. About 80% of the measured values are within a factor 2 of the computed value.

To use these expressions to evaluate the fundamental noise errors we have updated the instrument parameters like the background and source fluxes as they depend from the transmission and the emissivity of optics, the read-out-noise and the instrumental contrast measured in laboratory or on sky. To validate these estimates, we have observed in each mode a large number of calibrators with different magnitudes, selected from the MDFC catalogue [12] to be very likely centrosymmetric sources (hence with zero differential and closure phase) that can be modelled by a disc. The diameter of the calibrators is estimated from their color indexes and a correction is applied to the measured visibility. To remove the effect of the broad band errors, which are separately analyzed in the next two sections, we fit the measurement $m(\lambda)$ with a low order polynomial function $f(\lambda)$ adapted to the measurement behavior (usually a 2nd order function). Then we compute the measured standard deviation $\sigma_M(\lambda)$ of the residual $m(\lambda) - f(\lambda)$ and we plot the predicted and measured values on the same graph as illustrated in figures 2. We fine tune the instrumental parameters (mainly the actual transmission) to have a computed value going through the median of measured points. This adjusted transmission is in agreement with the transmission measured in laboratory combined with the estimated VLTI transmission within 50%. Then the adjusted computed fundamental noise error is used to predict this error for the measurement on any source given its coherent flux. This analysis has been made for all modes of MATISSE, for ATs and UTs.

On UTs we had much less commissioning time and we use systematically the smaller number of available measures to set the conversion factors between ATs and UTs. In L the conversion factor is of the order of 14, which is below the expected surface ratio of 20. This indicates that the NAOMI adaptive optics deliver a higher and/or more stable Strehl ratio than the UTs or that the UT Coude train needs to be recoated. In N the conversion factor is of the order of 30, which indicates that the background noise is higher on ATs than on UTs in spite of the fact that on a single mode instrument the solid angle on the sky is independent of the telescope diameter.

The agreement between the computed and measured precision is good at low flux but the measured precision reaches a plateau at high flux and stops to decrease when the source brightness increases. To account for that we add a flux independent variance to the computed variance, that sets a lower limit to the precision of measurements per minute of observation that is given in table 2 below.

Table 2. Best (i.e. minimum) values of MATISSE errors at high flux. For the differential phase, these values are given for a broad reference channel. For narrow continuum-line-continuum measurement in L, the differential phase can be as precise than0.2°.

Measure	**L**	**M**	**N**
Visibility	$3\ 10^{-3}$	$5\ 10^{-3}$	$3\ 10^{-3}$
Closure Phase	0.1°	0.2°	0.1°
Differential Phase	1°	1°	0.2°

The limits on the Visibility and Closure phase set a fundamental limit on the dynamical range of reconstructed images of the order of 300. Given the limited u-v coverage that can be expected with 4 telescopes, this limit will quite certainly never be approached with practical u-v coverages at the VLTI. The differential phase precision limit set a more severe limit on the detection of faint companions, of the order of 1/300 in L and M and 1/1500 in N. This limit is due to the imperfect calibration of the chromatic OPD, that is the next frontier in MATISSE calibration and data processing.

3.4 Instrumental visibility changes with seeing

The changes in seeing conditions and some instrumental features like transient telescope vibrations affect the instrument + atmosphere instrumental response. This is illustrated in figure 3 showing the variation of the instrument visibility with seeing and atmospheric coherence time τ_0.

The instrumental visibility has been estimated on calibrators and corrected from their diameter estimated from color indexes. The observations were made in the L band, from 3.1 to 3.9 µm with a frame time of DIT=75 ms. We see that the response is much more sensitive to τ_0 than to seeing and becomes little sensitive to atmospheric changes for $\tau_0 > 5\ ms \simeq DIT/15$.

So, the first impact of seeing changes is a variation of the coherent flux due to a loss in instrumental visibility that can exceed a factor 2 when we move from "fair" conditions ($\tau_0 > 5\ ms$) to bad conditions ($\tau_0 < 3\ ms$). All the limits given here are in coherent flux. The user must consider these changes in coherent flux and hence in performances when they define the seeing conditions required for their observations

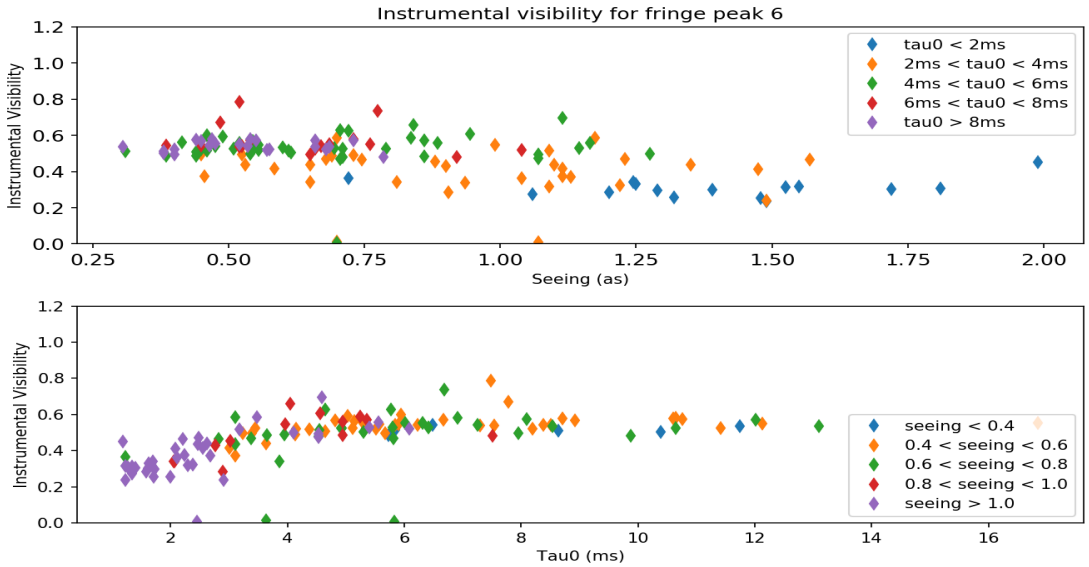

Figure 3. Variation of the instrument + atmosphere visibility as a function of seeing in arcseconds (top) and of the atmospheric coherence time in the visible in ms (bottom). In the top figure the colors also indicate the coherence time range, while in the bottom figure they indicate the seeing range. The observations were made in the L band, from 3.1 to 3.9 µm with a frame time of DIT=75 ms. As a wide range of magnitudes have been used, some measurements are sensitive also to fundamental noise, and to errors in calibrator diameter estimates and corrections.

3.5 Broad Band Calibration errors due to seeing changes

To evaluate the calibration errors due to seeing changes we have analyzed the so-called time transfer functions that show the variation of the broad-band measurements on bright calibrators as a function of time as illustrated in figure 4. Then, we mimic a "snapshot mode" calibration-science-calibration sequence or an "imaging mode" calibration based on a global fit through all the calibrators of a night. The two methods give very similar results that are summarized in the table below.

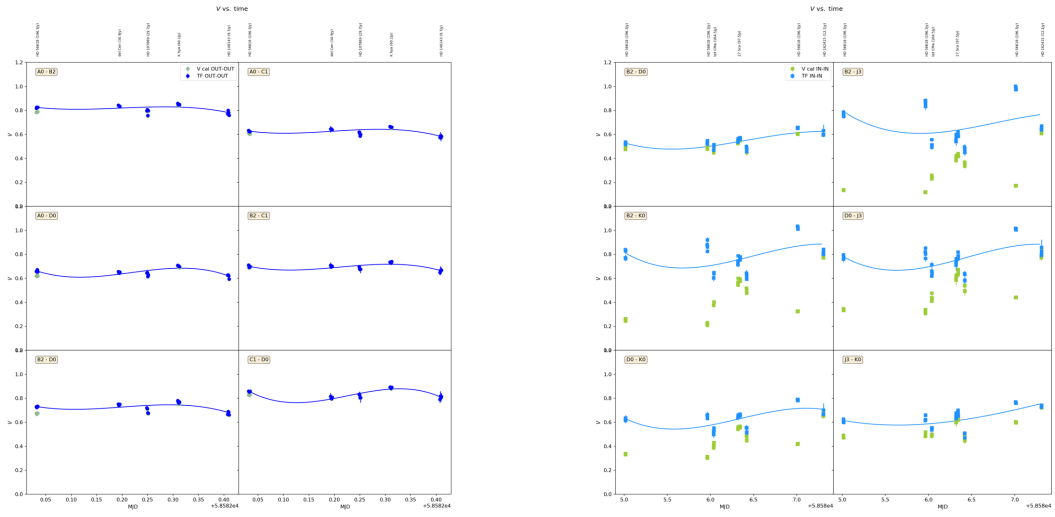

Figure 4. Example of visibility "transfer function" vs time, in L band at low resolution with ATs, for a good night (left, seeing=0.6as) and a bad night (right, seeing=1as). The blue dots are for calibrator visibility corrected from the calibrator diameter. The green dots are for raw visibility measurements. The rms of the difference between the measures and the fit is an estimate of the broad band calibration error.

Table 3. Broad band calibration errors on visibility and closure phase as a function of seeing conditions, for the standard frame times of MATISSE, 75 ms in L only, 111 ms in L&M and a 10 frames modulations cycle of 240 ms in N.

		L		M		N	
Seeing conditions		DIT=75 ms		DIT=111 ms		DIT.N_{mod}=240 ms	
τ_0 (ms)	**Seeing** (as)	Visibility	Closure Phase	Visibility	Closure Phase	Visibility	Closure Phase
3.2±0.5	0.96±0.1	0.08	0.30°	0.05	0.25°	0.045	1.75°
6.8±0.5	0.74±0.1	0.02	0.26°	0.020	0.24°	0.02	0.49°
7.5±0.5	0.56±0.1	0.02	0.16°	0.015	0.15°	0..015	0.29°

The closure phase numbers are given using the BCD calibration. A calibration using external calibrators only yields broad band closure phase errors between 1° and 2°.

3.6 Broad band photometric calibration errors.

To estimate the visibility from the coherent flux measurements, we need to separate the source and background contribution to the photometric measures. For all sources and N and M and for faint sources in L this needs telescope chopping. The broad band photometric errors produce an additional source flux dependent error. We have estimated it from statistics of the measured photometry for bins of calibrator with similar magnitudes. On ATs we have a data base allowing reliable statistics. On UTs dot have enough data and we assume that the photometric errors are the same as on UTs with of course a different conversion into source equivalent flux. From MIDI time we know that this is a pessimistic and conservative estimate for UTs that are less sensitive to chopping defects than the ATs. The actual measurements made with UTs confirm that we are quite certainly slightly overestimating the photometric noise with UTs.

The estimation of the noise on the photometric estimates due to the background fluctuations have been based on a statistical analysis of the sky frames obtained from telescope chopping, for the full L and M bands and 1 µm sub-bands in N.

Table 4. Broad band photometric errors given in equivalent source flux in Jy for all spectral bands (at 9 µm in N). The UTs values are deduced from the AT values using the measured UT/AT flux ratios.

	L	M	N
AT	0.11 Jy	0.19 Jy	2.3 Jy
UT	0.008 Jy	0.016 Jy	0.08 Jy

3.7 Bias on the coherent flux

In N band, below typically 20 Jy on ATs, the SNR on the coherent flux per spectral channel and coherence time becomes comparable or lower to one. Then, adding the squared modulus of the coherent flux becomes very inefficient as indicated in section 3.2. It is then necessary to perform a coherent integration of the complex coherent flux beyond the coherence time. This is done by an estimate of the global phase delay in each frame that is then corrected before direct addition. This is equivalent to shifting all fringes in individual frames to the same position before adding them in a long exposure. This improves quite substantially the sensitivity limit for all measures. However, errors on the estimation of the phase delay in each frame yield a bias on the coherent flux that stops to decrease proportionally to the source flux. When the phase delay is estimated on the N band data of the source itself, this bias limits to ~5 Jy at 8.5 µm (~8 Jy at 11 µm) the possibility to obtain reliable coherent fluxes as shown by figure 5.

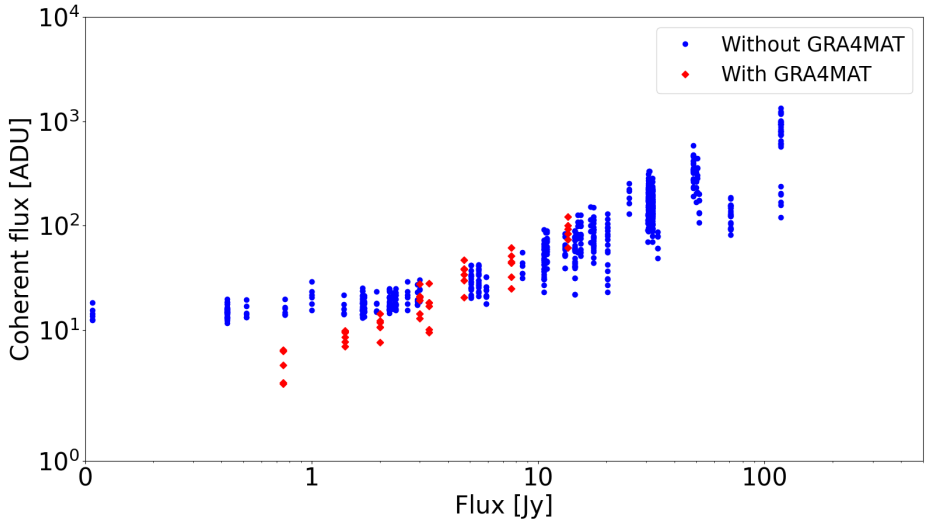

Figure 5. Measured coherent flux as a function of the source flux. The measures are made for 1mn exposures and averaged over a 1 µm spectral band. The blue dots are for a processing with phase delay estimates from the N band itself. They show a bias on the coherent flux for targets fainter than ~5 Jy. The red dots are for a processing with phase delays deduced from the GRA4Mat measures in the K band. Then the bias, if any, is below 1 Jy.

4. GLOBAL PERFORMANCES

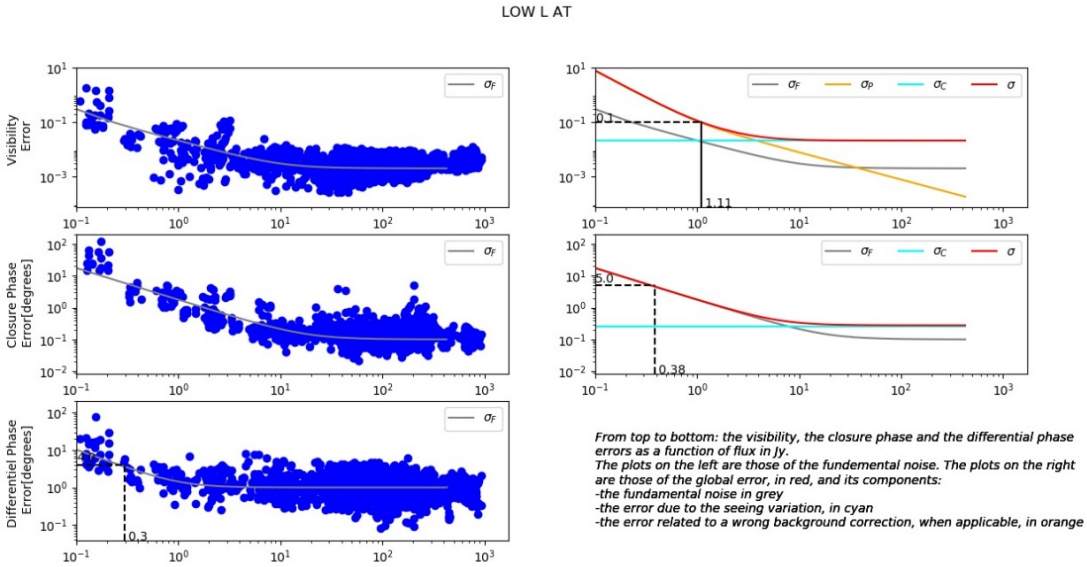

Figure 6. Illustration of the general performance of MATISSE in LR-L with ATs. In the left column we plot the measured fundamental noise per spectral channel (blue dots) as a function of the source coherent flux. The grey line shows the value of the computed precision that goes through the median of the measures. Visibility are on top in visibility units, Closure Phase is in the middle and Differential Phase is on bottom, in degrees. The coherent flux is in Jy. The top right panel shows the visibility fundamental noise standard deviation (grey), the flux dependent broad band photometric error (yellow) and the broad band calibration error due to seeing changes that is independent from the flux (cyan) as well as their combination (red) assuming these are independent variables.

4.1 Method

The figure 6 illustrates the global performance estimate of MATISSE that combines the different contributions to the MATISSE measurement errors. The left panels show the fundamental noise measures, fitted by the computed prediction for the visibility, the closure phase and the differential phase. For the differential phase, we measure directly the precision on the fundamental noise plot, and this gives the precision on the differential phase between one channel and a nearby reference channel or a broad reference channel if this has been correctly corrected from chromatic OPD. The actual differential phase accuracy in that latest case remains an open issue.

For the closure phase we add the variance of the fundamental noise per channel and the broad band calibration error deduced from the time transfer function of the measure as described in section 3.5. Then the plot of these combined variances is used to find the coherent flux that yields a closure phase accuracy per spectral channel better than 5° in 50% of the cases.

For the absolute visibility we add the variances of the fundamental noise errors, the seeing broad band calibration error and the photometric broad band calibration error and use the plot of the combined variance to find the coherent flux that yields a visibility accuracy per spectral channel better than 0.1 in 50% of the cases. This has been done for UTs and ATs and for all spectral set-ups.

4.2 Validation

To check the overall validity, we have plotted the broadband measured visibility as a function of the flux, as illustrated in figure 7 on LR-N. We see clearly the flux independent regime above 30 Jy in that mode. The rms value in that regime is between 0.02 and 0.03 and gives the calibration error for a science target calibrated by a calibrator obtained at any moment, including in a different night. In N band this is possible when we use the short 20 ms frames individually (on bright enough sources) because that frame time is much shorter than the coherence time in N. Globally and except at very low fluxes (which are below the limit that we offer for that observation and that mode) almost all points are within the ±1 σ interval of our global performance estimation.

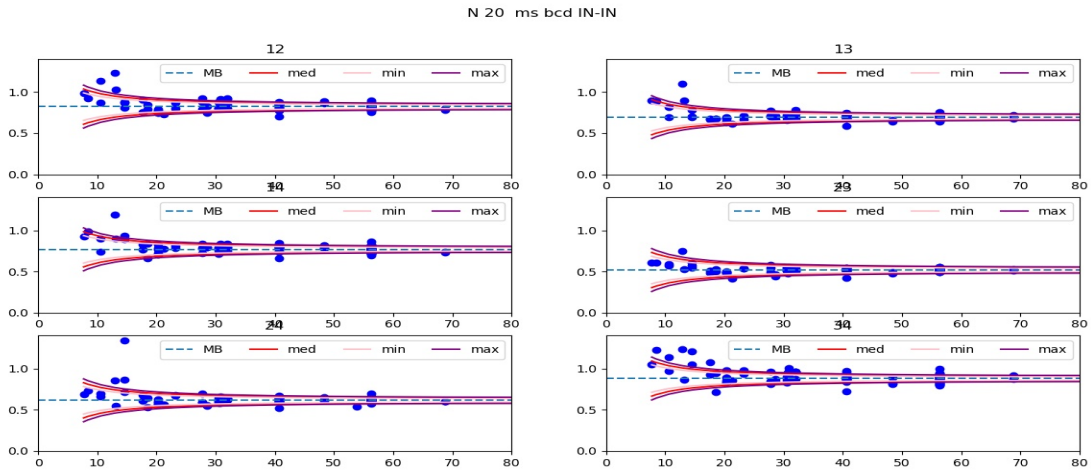

Figure 7. Measured instrument + atmosphere visibility as a function of the source flux (blue dots), here in LR-N averaged between 8 and 9 μm, with the ATs. The dashed horizontal line in the mean instrument visibility that ranges from 0.6 to 0.9 according to the baseline. The red lines are the mean ±1 median sigma. The yellow and brown lines correspond to the best and the poorest observing conditions. The limiting coherent flux for a 0.1 visibility accuracy is 17 Jy for that mode and spectral band. Above that limit, almost all experimental points are within ±1σ.

4.3 The current performances of MATISSE standalone

The table 5 below summarizes the current flux limits to obtain, per spectral channel and per mn of observation, a visibility accuracy better than 0.1, a closure phase accuracy better than 5° and a differential phase precision better than 4°. For all modes but for the LR in N, the differential phase precision of 4° correspond to a coherent flux SNR of 10. In LR-N we have also to consider the coherent flux bias that sets a lower flux for its use. The values given in table 5 are for good and

fair seeing conditions, i.e. seeing<0.9 arcseconds and τ_0>4 ms. When the seeing conditions are poor (τ_0<3 ms), the coherent flux can lose up to 1 magnitude and all limits in table 5 move up by typically 2 Jy.

Table 5. MATISSE sensitivity limits defined has the lowest flux in Jy allowing to achieve a visibility accuracy of 0.1, a closure phase accuracy of 5°, a differential phase precision of 4° and a coherent flux SNR of 10.

Telescope	Resolution	Visibility			Closure Phase			Differential Phase			CF bias limit	
		L	**M**	**N**	**L**	**M**	**N**	**L**	**M**	**N**	**N1**	**N2**
ATs	Low	1.1	2.1	16.8	0.4	1.9	9.4	0.3	1.1	2	5	8
	Medium	3.8	16	-	3.3	15.6	-	2.4	11	-	-	-
	High	20.1	-	30.3	14.7	-	29.9	10.8	-	25.3	5	8
UTs	Low	0.3	0.4	0.9	0.07	0.2	0.3	0.06	0.15	0.07	0.3	0.5
	Medium	1.1	1.1	-	0.8	0.9	-	0.6	0.7	-	-	-
	High	2.4	-	1.6	1.7	-	1.5	1.2	-	1.1	0.3	0.5

The limits in table 5 are given for the center of the bands as described in table 6. Near the band edges the measurement errors can be quite larger, particularly on the differential phase that also partially contaminates the closure phase, through cross-talks between baselines and the visibility through the inclination of the fringes.

Table 6. Spectral band used to define the measurement performances given in table 5.

resolution	**L**	**M**	**N & N1**	**N2**
Low	3.5±0.3 µm	4.75±0.2 µm	8.5±0.5 µm	10.5±0.5 µm
Medium	0.2 in [3.1-4.2] µm	0.2 in [4.5-5] µm	Does not exist	Does not exist
High	0.1 in [3.8-4.2] µm	Does not exist	In [8-9] µm	In [10-11] µm

5. THE GRA4MAT AND VHR EXTENSIONS

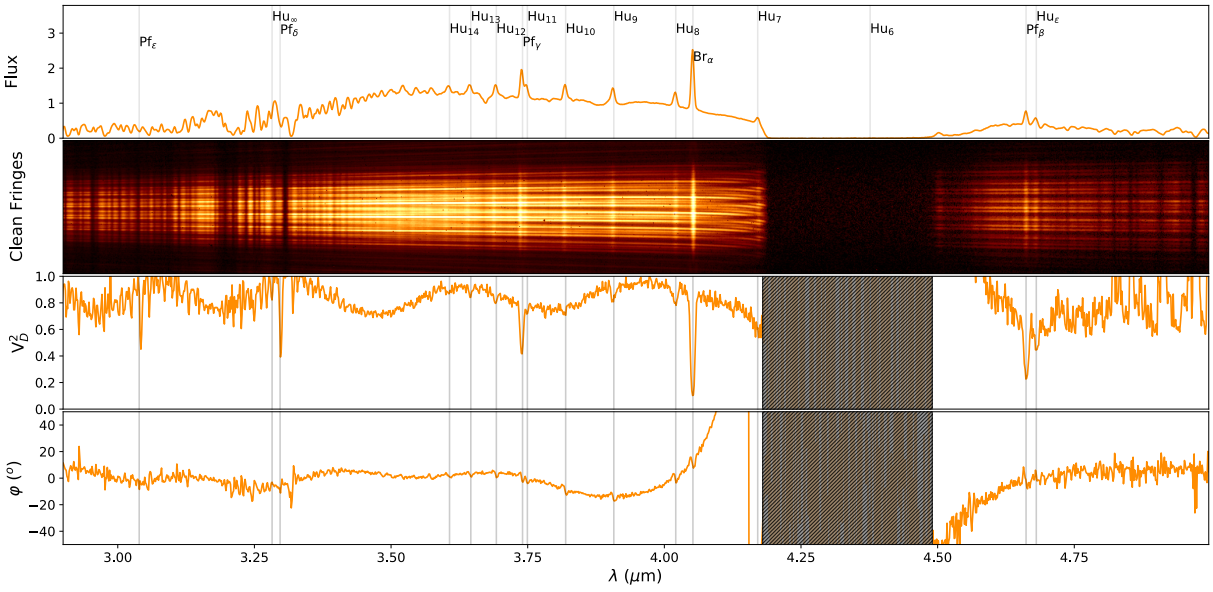

Figure 8. MATISSE MR-LM observations in the GRA4MAT mode with a fringe stabilization with the Gravity Fringe Tracker. The central images show the interferometric channel of MATISSE with a 10 s frame time with straight and stable high contrast fringes from 3.9 to 4.9 µm and a collection of bright emission lines and darks telluric absorption lines. The upper plot is the source spectrum showing a rich collection of hydrogen emission lines in Brα and the Humphrey and Pfund series. The second to bottom plot show the measured visibility and the bottom plot shows the differential phase.

In late 2019 we started commissioning simultaneously the Very High-Resolution mode of MATISSE (R~3400 in L and M, from 3.85 to 4.9 μm) and the GRA4MAT mode, that is the use of the GRAvity fringe tracker FOR the stabilization of MATISSE fringes.

Without GRA4MAT, the VHR mode gives access to 0.025 μm spectral windows for sources brighter than 40 Jy in L and 55 Jy in M with ATs. This is a very limited range of application, and the VHR mode on ATs is and will remain offered only in association with fringe tracking with GRA4MAT.

The GRAVITY Fringe Tracker is operated in the K band and that sets specific limits for the coherent magnitude in K that are given in table 7.

Table 7. K band coherent magnitude limit for GRA4MAT operation. Note that the seeing bins in that table are the standard ESO ones, while the seeing bins used in the MATISSE tables above are from actual but more limited statistics on our data.

Conditions	**Good (T≤10%)**	**Fair (T≤50%)**	**Poor (T≤85%)**
Seeing and τ_0	Sg ≤0.6"; τ_0 >5.2 ms	Sg ≤1.0"; τ_0 >3.2 ms	Sg ≤1.4"; τ_0 >1.6 ms
K coherent limit	8.5	7.5	6.5

Within these limits GRA4MAT allows long exposures in L&M that enable reading the full detector and hence accessing simultaneously the full MATISSE spectral coverage. The Figure 8 illustrates this on the Be binary star delta Cen, which shows the very rich information that can be extracted from a single shot broad band observation at medium or high spectral resolution. We can observe simultaneously many emission lines, each showing differential visibility and differential phase signatures that constrain, respectively, the size, the kinematics and the asymmetry of the gas envelope. The small oscillations of the visibility in the continuum reveal the faint companion of delta Cen. This figure also illustrates the strong effect of chromatic OPD near the band limits. This has a strong impact on the differential phase and a careful modeling and calibration of that chromatic OPD will be needed to push the continuum differential phase accuracy below the current 1° accuracy. This chromatic OPD has also an attenuated but real impact on the visibility and closure phase that limits the current dynamics of MATISSE to about 300. The analysis and calibration of the differential phase should allow modeling and correcting these effects and hence increasing the capability of MATISSE to characterize fainter companions. We can also analyze the many telluric lines that can be seen between 3 and 3.5 μm and between 4.7 and 5 μm, which have a masked impact on the accuracy of broad band measures at lower resolutions.

The second advantage of observations with GRA4MAT is that it strongly reduces the piston jitter seen by MATISSE and hence strongly stabilizes the instrument visibility, that becomes nearly unsensitive to seeing, within the operation limits of GRA4MAT.

The last and main advantage of GRA4MAT is the strong gain in sensitivity of higher spectral resolution observations in L and M that is displayed in table 8.

Table 8. Limits in Jy to achieve differential phase precision of 4° and a coherent flux SNR=10 and a closure phase accuracy of 5°, per spectral channel and per 1 mn exposure.

		L		**M**	
Resolution	DIT	**Coherent flux & Differential phase**	**Closure phase**	**Coherent flux & Differential phase**	**Closure phase**
LR	DIT=1s	0.17	0.25	0.7	1
MR	DIT=10s	1	1.5	11	15.6
HR	DIT=10s	2	3	--	--
VHR	DIT=10s	20	25	17	25

The absolute visibility accuracy remains limited by the precision of the photometric measures that is not improved by GRA4MAT. Moreover, the first implementation of GRA4MAT did not permit chopping while fringe tracking. As chopping is necessary for accurate visibility in L and in M, the provisional procedure currently offered combines MATISSE standalone observations at low resolution with chopping and without GRA4MAT, that give the best absolute visibility measures, with GRA4MAT observations at higher spectral resolution that give the performances in table 8 for the other measures. The operation of GRA4MAT with chopping is possible since March 2020, but the covid-19 crisis delayed its full commissioning. It should be offered after April 2021.

The last and not least advantage of GRA4MAT is that in the N band it allows coherent integration of frames [13]. The phase delay and group delay in the K band given by the GRAVITY fringe tracker allow computing the chromatic phase difference between K and N [14] and then measuring the phase delay in N with an accuracy better than 0.2 rad. This makes the coherent flux bias lower than the fundamental noise limits, as illustrated in figure 5. The SNR=10 coherent flux limit with MATISSE is then identical to the differential phase precision limit=4° given in table 5, i.e. 2 Jy with ATs.

6. CONCLUSION

The performances of MATISSE described in this paper have been established on a solid statistical basis, in particular with ATs and we consider the numbers as quite reliable. The high accuracy achieved almost always in closure phases and in fair and good seeing on visibility will be strongly constraining on the adjustment of models. During the December 2018 "imaging" commissioning run we have been able to obtain images during the run itself. Of course the images obtained later after a careful data processing and calibration were of much higher quality but it is quite remarkable that, with some good expertise of MATISSE image reconstruction tools (that can be acquired in a couple of weeks), it is possible to evaluate the imaging quality of the data and for example the completeness of the u-v coverage in the hours that follow the end of each night.

One of the specifications of MATISSE is that it should achieve in the N band the same data quality than the first-generation instrument MIDI. As showed by the numbers given in this paper and by several science examples in [5] and [8] this has been fully achieved, for each baseline for visibility and coherent flux, with the advantage that MATISSE obtains 6 baselines and one and gives closure phases for the first time in the L,M and N bands. The sensitivity of MATISSE in the L band will be a game changer for the study of AGNs as it dramatically increases the number of AGNs of observable AGNs.

The commissioning of MATISSE and in particular of GRA4MAT with UTs is not complete. It should be executed as soon as the covid-19 crisis makes it possible. The preliminary investigations of this mode in March 2020, just before the shutdown of Paranal showed that this mode will work but with a smaller gain than with ATs, in particular because of the instability of MACAO that is likely to limit the frame time to 1s.

Three points need deeper investigation to find the final performances of MATISSE. The first one is the calibration of the effects of the chromatic OPD on the differential phase. The fundamental noise limits on the differential phase are well below 0.1° and the current limit is of 1° in L and M for local differential phase and up to 5° near the band limits. A correct calibration of the differential phase in LR would open the way for chromatic imaging algorithms that use the differential phase and the coherent flux instead of the visibility and closure phase. this would extend the possibility to make N band images by 1 to 2 magnitudes. The new image reconstruction algorithms are the second development axis. Finally, it appears that the main limitation of MATISSE with the current VLTI will be the sensitivity of the Adaptive Optics. MATISSE will be a major benefactor of the GRAVITY+ upgrade of the adaptive optics on UT as well as of the possibility to use off-axis guide stars for fringe tracking on UTs and ATs with the separation of up to 40 as accessible in the N band.

REFERENCES

[1] Xavier Haubois, et al, "VLTI status update: tapping into a powerful second-generation instrumentation," Proc. SPIE 11446, (2020).

[2] Frank Eisenhauer, "A new era of interferometry with GRAVITY," Proc. SPIE 11443, (2020).

[3] Gravity collaboration et al, "First light for GRAVITY: Phase referencing optical interferometry for the Very Large Telescope Interferometer," Astronomy & Astrophysics 602, (2017).

[4] Bruno Lopez, et al, "MATISSE: perspective of imaging in the mid-infrared at the VLTI," Proc SPIE 7013, (2008).

[5] Bruno Lopez, et al, "MATISSE, the VLTI mid-infrared imaging spectro-interferometer," submitted to Astronomy & Astrophysics, (2021).

[6] Florian Kirchschlager, et al, "First L band detection of hot exozodiacal dust with VLTI/MATISSE," Monthly Notices of the Royal Astronomical Society: Letters, Volume 499, Issue 1, pp.L47-L52 (2020).

[7] Jozsef Varga, et al, "The asymmetric inner disk of the Herbig Ae star HD 163296 in the eyes of VLTI/MATISSE: evidence for a vortex?," to appear in Astronomy & Astrophysics, (2021).

[8] Florentin Millour, et al, “Science with MATISSE,” Proc. SPIE 11446, (2020).

[9] Romain G. Petrov, et al, “AMBER, the near-infrared spectro-interferometric three-telescope VLTI instrument,” Astronomy and Astrophysics 464(1), 1-12 (2007).

[10] Florentin Millour, et al, “AMBER closure and differential phases: accuracy and calibration with a beam commutation,” Proc SPIE 7013, (2008).

[11] Alexis Matter, et al, “Parasitic interference in classical and nulling stellar interferometry,” Proc SPIE 8445, (2012).

[12] Pierre Cruzalèbes, et al, “A catalogue of stellar diameters and fluxes for mid-infrared interferometry,” Monthly Notices of the Royal Astronomical Society 490(3), 3158-3176 (2019).

[13] Philippe Berio, et al, “A posteriori co-phasing of N band MATISSE fringes with the fringe tracker GRA4MAT,” in preparation for Astronomy & Astrophysics, (2021).

[14] Chris Koresko, et al, “Water vapor measurement and compensation in the near- and mid-infrared with the Keck Interferometer Nuller,” Proc SPIE 6268, (2006).